Acoust Aust (2016) 44:343–357
DOI 10.1007/s40857-016-0065-4

ORIGINAL PAPER

2D Acoustic Design Sensitivity Analysis Based on Adjoint Variable Method Using Different Types of Boundary Elements

Leilei Chen[1] · **Linchao Liu**[1] · **Wenchang Zhao**[2] · **Haibo Chen**[2]

Received: 24 March 2016 / Accepted: 29 June 2016 / Published online: 14 July 2016

Abstract Continuous linear and quadratic boundary elements are often applied to numerical solution. Discontinuous higher-order boundary elements are developed for 2D acoustic problems to achieve higher accuracy in this paper. The Burton–Miller formulation is used to overcome the fictitious frequency problem when using a single Helmholtz boundary integral equation for exterior boundary-value problem. The strong singular integrals in Burton–Miller formulation using different types of element discretization are evaluated explicitly and directly, respectively. An example of scattering by an infinite rigid cylinder is presented to compare the performance of different types of elements. The effect of the position of nodes on the performance of discontinuous elements is studied, and an empirical value for optimal nodal position is concluded in this paper. Adjoint variable method is applied to evaluate the sensitivity value of the objective function, and the method of moving asymptotes is used for structural optimization analysis of noise barrier.

Keywords Discontinuous boundary element · Shape sensitivity analysis · Adjoint variable method · Structural optimization analysis

1 Introduction

Optimization algorithms can be categorized in many ways. One technique is dividing optimization algorithms into direct and approximate methods [1]. Direct methods, such as genetic algorithms and simulated annealing, are based on a clever choice of parameter variations to determine a global minimum. Examples for genetic algorithms and simulated annealing are discussed in [2,3] and [4,5], respectively. Both examples are applied to optimization problems in structural acoustics. Direct methods frequently find a global minimum but require a large number of function evaluations. By contrast, approximate methods converge with fewer function evaluations may also only converge to local minimum. Distinguishing global, mid-range, and local approximations is reasonable among approximation concepts. These categories comprehend local and global approximations, whereas the gap between the two is filled by mid-range approximation. Local approximation assumes that the approximation is only valid within the vicinity of one point in the design space, whereas global approximation is valid in the entire design space or at least in a large region of the entire space. Mid-range approximation attempts to utilize the strengths of local and global approximations and typically covers a larger range of the design space than local methods. A good review of these concepts is found in the doctoral thesis of van Houten [6], and a discussion is also provided in [1]. Local approximation methods also apply sensitivity information (i.e. gradient information) although global and mid-range methods can particularly benefit from such information. Most local approximation methods are based on a Taylor series approximation of the objective function within the vicinity of a certain design point (i.e. parameter set). First-order methods

✉ Leilei Chen
chenllei@mail.ustc.edu.cn

[1] College of Civil Engineering, Xinyang Normal University, Xinyang 464000, Henan, People's Republic of China

[2] CAS Key Laboratory of Mechanical Behavior and Design of Materials, Department of Modern Mechanics, University of Science and Technology of China, Hefei 230026, Anhui, People's Republic of China

use gradient information, whereas second-order methods use the Hessian in addition to gradient information. A comparison between the results of a structural acoustic optimization problem with seven different optimization methods using a local approximation is found in [7]. The latter and other older applications in structural acoustics [8–11] indicate that gradient information is provided using global finite differences that require at least one function evaluation per parameter to evaluate the entire gradient. This evaluation is easy to implement and therefore, has been widely used. Semi-analytic and analytic sensitivity analyses are distinguished in addition to global finite differences. These categorizations have been sufficiently reviewed and discussed by Haftka and Adelmann [12], see also [1,13]. Analytic and semi-analytic sensitivity analyses are significantly more accurate than global finite differences and typically require less computational costs. Analytic sensitivity analysis, which has been used as a direct differentiation method in recent years, is applied to structural acoustic problems[14–16]. Another development, particularly for problems with many design variables, becomes possible using an adjoint operator approach that has already been applied to structural acoustic problems [17,18]. Aside from local approximation, an acoustic design sensitivity analysis also provides information on the effect of a parameter on the acoustic performance of a given structure. In this paper, adjoint variable method is applied to evaluate the shape sensitivity of the objective function, and MMA method is used for optimization analysis of noise barrier.

Constant discretization is widely used for the numerical solution of acoustic BEM [14,15,19–21]. Discontinuous elements with higher accuracy are investigated in [22–26]. Error dependence in terms of frequency, element size, and location of nodes on discontinuous elements is presented by Marburg [24], and the result that discontinuous boundary elements perform more efficiently than continuous ones is also obtained in [24]. However, the research on the sensitivity analysis cannot be seen in these papers. In this paper, discontinuous higher-order boundary elements are developed for the acoustic shape sensitivity analysis to achieve higher accuracy. For discontinuous boundary elements, interpolation nodes are located inside the elements and the expressions of the interpolation functions are dependent on the position of the node inside the elements. So, different computing accuracy can be obtained by setting different nodal position. The major part of the paper consists of the investigation of the computational example of scattering from an infinite cylinder. For that, the numeric solution is compared with the analytic solution. The performance of different types of boundary elements is presented and compared, and the optimal values of the nodal position are also obtained in this paper.

On the other hand, the implementation of a single Helmholtz boundary integral equation may have the difficulty of non-uniqueness for exterior boundary-value problems. Burton–Miller method [27] which consists of a linear combination of the conventional boundary integral equation (CBIE) and its normal derivative equation (NDBIE) is used to overcome this problem. The NDBIE is hypersingular when the boundary is non-smooth, and some special treatments should be employed in its numerical evaluation. In this paper, the singular integrals in Burton–Miller formulation for different types of element discretization are evaluated explicitly and directly using Cauchy principal value and the Hadamard finite part integral method, respectively.

This paper is organized as follows. The 2D BEM formulations in acoustic state analysis and acoustic design sensitivity analysis are introduced in Sects. 2 and 3. In Sect. 4, numerical examples are presented to demonstrate the efficiency and validity of the proposed algorithm. Section 5 concludes the paper with further discussions.

2 2D BEM Formulation

Consider the following Helmholtz equation governing time-harmonic acoustic wave fields:

$$\nabla^2\phi(x) + k^2\phi(x) = 0, \quad \forall x \in \Omega, \tag{1}$$

where ϕ is the acoustic pressure with harmonic time dependence $e^{-i\omega t}$, i the imaginary unit, $k = \omega/c$ the wave number, ω the angular frequency, and c the wave speed in the acoustic medium Ω.

The integral formulation of the solution to the Helmholtz equation is

$$\phi(x^j) = \int_S G(x^j, x)q(x)\mathrm{d}S(x) - \int_S F(x^j, x)\phi(x)\mathrm{d}S(x), \quad x^j \in \Omega, \tag{2}$$

where x^j is the source point, x the field point and $G(x^j, x)$ the Green's function. For two-dimensional problem, the Green's function is given by

$$G(x^j, x) = \frac{\mathrm{i}}{4}H_0^{(1)}(kr), \tag{3}$$

and

$$F(x^j, x) = \frac{\partial G(x^j, x)}{\partial n(x)} = -\frac{\mathrm{i}k}{4}H_1^{(1)}(kr)\frac{\partial r}{\partial n(x)}, \tag{4}$$

where $r = \mid x - x^j \mid$, $H_n^{(1)}$ denotes the first kind Hankel function of the n-th order. The derivative of Eq. (2) with respect to the outward normal at point x^j can be expressed as

$$q(x^j) = \int_S G^1(x^j, x) q(x) \mathrm{d}S(x) - \int_S F^1(x^j, x) \phi(x) \mathrm{d}S(x), \tag{5}$$

where

$$G^1(x^j, x) = \frac{\partial G(x^j, x)}{\partial n(x^j)} = -\frac{\mathrm{i}k}{4} H_1^{(1)}(kr) \frac{\partial r}{\partial n(x^j)}, \tag{6}$$

and

$$F^1(x^j, x) = \frac{\partial F(x^j, x)}{\partial n(x^j)} = \frac{\mathrm{i}k}{4r} H_1^{(1)}(kr) n_l(x^j) n_l(x) + \frac{ik^2}{4} H_2^{(1)}(kr) \frac{\partial r}{\partial n(x^j)} \frac{\partial r}{\partial n(x)}, \tag{7}$$

n_l is the Cartesian component of $n(x^j)$ or $n(x)$. $\frac{\partial r}{\partial n} = r_{,l} n_l$, where an index after a comma denotes the partial derivative with respect to the coordinate component, such as $r_{,l} = \partial r / \partial x_l$. Einstein's summation convention is used throughout the paper, so repeated indices imply a summation over their range.

When the source point x^j in Eqs. (2) and (5) is close to the boundary S, we can get the following boundary integral equations:

$$c(x^j)\phi(x^j) = \int_S G(x^j, x) q(x) \mathrm{d}S(x) - \int_S F(x^j, x) \phi(x) \mathrm{d}S(x), \tag{8}$$

and

$$c(x^j) q(x^j) = \int_S G^1(x^j, x) q(x) \mathrm{d}S(x) - \int_S F^1(x^j, x) \phi(x) \mathrm{d}S(x), \tag{9}$$

where the coefficient $c(x^j)$ is determined by the boundary geometry at the source point x^j. Equations (8) and (9) are referred to as the CBIE and NDBIE formulas. It is well-known that the CBIE or NDBIE for exterior boundary-value problems may have difficulty of non-uniqueness. However, the linear combination of them can yield unique solutions for all frequencies, when the coupling constant of the two equations is a complex [28]. If the boundary is non-smooth, Eq. (8) is a strong singular boundary integral equation and Eq. (9) is a hypersingular boundary integral equation. Such integrals usually need special treatments, but they can be evaluated explicitly and directly with the Cauchy principal value and the Hadamard finite part integral method respectively, please see Appendix 1 for the details of the deduction process.

If the boundary S is divided into N elements, one can obtain the following system of linear algebraic equations:

$$[H]\{\phi\} = [G]\{q\}. \tag{10}$$

Moving all the unknown terms of Eq. (42) to the left-hand side and all the known terms to the right-hand side by considering the boundary conditions (e.g. for Neumann type problems, the pressure ϕ is unknown and the normal derivative q is specified), one finally obtain the following system of linear equations:

$$[A]\{x\} = \{b\}, \tag{11}$$

where $[A]$ is the coefficient matrix, $\{x\}$ the vector of unknown boundary values at the nodes, and $\{b\}$ the known vector. All the unknown boundary state values can be obtained after Eq. (11) is solved. Finally, one can calculate the sound pressure ϕ at any interior point using Eq. (2).

A well-known disadvantage for directly solving the above equation is that the coefficient matrices $[H]$ and $[G]$ are dense and non-symmetrical, which induce $O(N^2)$ arithmetic operations when dealing with a problem with N unknowns. The fast multipole method (FMM) accelerates the solution of the conventional boundary element system of equations and decreases the memory requirement [14,15,19]. The main idea of FMM is to approximate the fundamental solution for BEM in terms of spherical Hankel functions, Legendre polynomials, and plane waves. The coefficient matrices consist of two parts. One is the near-field part, which is evaluated by integration in the usual way in the vicinity of the source point. The other is the far-field part, which is not directly computed. Applying FMM on a hierarchy of clusters reduces the complexity of BEM from $O(N^2)$ to $O(N \log N)$. FMM has two forms. One is the original FMM (low-frequency method) based on a series expansion formula of the fundamental solution; the other is the diagonal form FMM (high-frequency method) based on a plane wave expansion formula of the fundamental solution. The original FMM is inefficient for high-frequency problems, and the diagonal form FMM has instability problems for the solution of low-frequency Helmholtz equations. However, the wideband FMM obtained by combining the original FMM and the diagonal form FMM can be used to overcome these difficulties [19,21]. Detailed information about the wideband FMM algorithm can be found in[19,21].

3 Sensitivity Analysis Based on Adjoint Variable Method

Acoustic design sensitivity analysis can provide insights into the effects of geometric changes on the acoustic performance

of the given structure and thus, this analysis is important to the acoustic design and optimization processes. Without loss of generality, the objective function W can be defined as follows:

$$W = \int_S w_1(\phi, q)\mathrm{d}S + \int_\Omega w_2(\phi)\mathrm{d}\Omega, \tag{12}$$

where w_1 is an arbitrary continuous function of sound pressure and its normal derivative, and w_2 is an arbitrary continuous function of sound pressure in the acoustic domain. By differentiating the above equation with respect to the design variable ϑ, the first-order sensitivity of the objective function can be obtained as follows:

$$\begin{aligned}\frac{\partial W}{\partial \vartheta} = &\int_S \frac{\partial w_1}{\partial \phi}\frac{\partial \phi}{\partial \vartheta}\mathrm{d}S + \int_S \frac{\partial w_1}{\partial q}\frac{\partial q}{\partial \vartheta}\mathrm{d}S + \int_S w_1 \frac{\partial \mathrm{d}S}{\partial \vartheta} \\ &+ \int_\Omega \frac{\partial w_2}{\partial \phi}\frac{\partial \phi}{\partial \vartheta}\mathrm{d}\Omega + \int_\Omega w_2 \frac{\partial \mathrm{d}\Omega}{\partial \vartheta}.\end{aligned} \tag{13}$$

According to [17], the derivatives of the boundary and domain element are respectively given by

$$\frac{\partial \mathrm{d}S}{\partial \vartheta} = \left[\frac{\partial^2 x_l}{\partial \vartheta \partial x_l} - \frac{\partial^2 x_l}{\partial \vartheta \partial x_j} n_l(x) n_j(x)\right]\mathrm{d}S, \tag{14}$$

$$\frac{\partial \mathrm{d}\Omega}{\partial \vartheta} = \frac{\partial^2 x_l}{\partial \vartheta \partial x_l}\mathrm{d}\Omega, \tag{15}$$

where $\frac{\partial x_l}{\partial \vartheta}$ will be evaluated when the boundary of the analysed domain is fully parameterized with the design variable. Directly using Eq. (13) to evaluate the sensitivity of the objective function, it seems essential to know all sensitivity values of pressure ϕ and normal derivative q. Actually, when directly differentiating Eqs. (8) and (9) with respect to the design variable and then solving the combined differentiation equation, the sensitivity values of nodal pressure and normal derivative can be obtained. But the combined differentiation equation depends on the design variable ϑ. Consequently, m design variables ϑ_j with $j = 1, 2, ..., m$ will produce m sensitivity equation, and thus the linear system of equations needs to be solved for m times, which is very time consuming. For a large number of design variables, adjoint variable method performs more efficiently than direct differentiation method. During the analysis of adjoint variable method, the unknown sensitivity values of sound pressure and normal derivative are eliminated from the sensitivity equations of the objective functions by introducing certain adjoint equation depending on the objective function, but not the design variables.

In order to eliminate the unknown sensitivity values of nodal sound pressure and normal derivative on the boundary, a constraint condition is added to the objective function W to form an augmented function as follows:

$$\begin{aligned}\bar{W} = W + R = &\int_S w_1(\phi, q)\mathrm{d}S + \int_\Omega w_2(\phi)d\Omega \\ &+ \int_\Omega \gamma(x)\left[\nabla^2\phi(x) + k^2\phi(x)\right]\mathrm{d}\Omega.\end{aligned} \tag{16}$$

Actually $\bar{W}$ is identical to W because the equation $\nabla^2\phi(x) + k^2\phi(x) = 0$ is always satisfied in the domain. By using the Green's first identity, the constraint condition R can be expressed as

$$\begin{aligned}R = &\int_S \gamma(x)q(x)\mathrm{d}S - \int_\Omega \gamma_{,l}(x)\phi_{,l}(x)\mathrm{d}\Omega \\ &+ \int_\Omega k^2\gamma(x)\phi(x)\mathrm{d}\Omega.\end{aligned} \tag{17}$$

By differentiating the above equation with respect to design variable and using Green's first identity again, the sensitivity formulation of R can be derived by

$$\begin{aligned}\frac{\partial R}{\partial \vartheta} = &\int_S \gamma(x)\frac{\partial q(x)}{\partial \vartheta}\mathrm{d}S - \int_S \frac{\partial \gamma(x)}{\partial n}\frac{\partial \phi(x)}{\partial \vartheta}\mathrm{d}S \\ &+ \int_S \gamma(x)q(x)\frac{\partial \mathrm{d}S}{\partial \vartheta}.\end{aligned} \tag{18}$$

By combining Eqs. (13) and (18), we can obtain the sensitivity formulation of the objective function $\bar{W}$, as follows

$$\begin{aligned}\frac{\partial \bar{W}}{\partial \vartheta} = &\int_S \left(\frac{\partial w_1}{\partial \phi} - \frac{\partial \gamma}{\partial n}\right)\frac{\partial \phi}{\partial \vartheta}\mathrm{d}S + \int_S \left(\frac{\partial w_1}{\partial q} + \gamma\right)\frac{\partial q}{\partial \vartheta}\mathrm{d}S \\ &+ \int_S (w_1 + \gamma q)\frac{\partial \mathrm{d}S}{\partial \vartheta} \\ &+ \int_S \left(\gamma_{,j}q + \frac{\partial \gamma}{\partial n}\phi_{,j} - \gamma_{,l}\phi_{,l}n_j + k^2\gamma\phi n_j\right)\frac{\partial x_j}{\partial \vartheta}\mathrm{d}S \\ &+ \int_\Omega w_2 \frac{\partial \mathrm{d}\Omega}{\partial \vartheta} \\ &+ \int_\Omega \left(\gamma_{,ll} + k^2\gamma + \frac{\partial w_2}{\partial \phi}\right)\frac{\partial \phi}{\partial \vartheta}\mathrm{d}\Omega \\ &- \int_\Omega \left(\gamma_{,ll} + k^2\gamma\right)\phi_{,j}\frac{\partial x_j}{\partial \vartheta}\mathrm{d}\Omega,\end{aligned} \tag{19}$$

where the adjoint equation can be defined as

$$\nabla^2\gamma + k^2\gamma + \frac{\partial w_2}{\partial \phi} = 0, \qquad \forall x \in \Omega. \tag{20}$$

According to the following boundary conditions

$$\frac{\partial \gamma}{\partial n} = \frac{\partial w_1}{\partial \phi}, \qquad x \in S_q, \tag{21}$$

$$\gamma = -\frac{\partial w_1}{\partial q}, \qquad x \in S_\phi. \tag{22}$$

By substituting Eqs. (20)–(22) into Eq. (19), we can obtain the following formulation

$$\begin{aligned}\frac{\partial \bar{W}}{\partial \vartheta} &= \int_{S_\phi}\left(\frac{\partial w_1}{\partial \phi}-\frac{\partial \gamma}{\partial n}\right)\frac{\partial \phi}{\partial \vartheta}\mathrm{d}S+\int_{S_q}\left(\frac{\partial w_1}{\partial q}+\gamma\right)\frac{\partial q}{\partial \vartheta}\mathrm{d}S\\ &+\int_S\left(\gamma_{,j}q+\frac{\partial \gamma}{\partial n}\phi_{,j}-\gamma_{,l}\phi_{,l}n_j+k^2\gamma\phi n_j\right)\frac{\partial x_j}{\partial \vartheta}\mathrm{d}S\\ &+\int_S\left(w_1+\gamma q\right)\frac{\partial \mathrm{d}S}{\partial \vartheta}+\int_\Omega\frac{\partial w_2}{\partial \phi}\phi_{,j}\frac{\partial x_j}{\partial \vartheta}\mathrm{d}\Omega\\ &+\int_\Omega w_2\frac{\partial \mathrm{d}\Omega}{\partial \vartheta}.\end{aligned}\tag{23}$$

Also, we have

$$\begin{aligned}&\int_\Omega\frac{\partial w_2}{\partial \phi}\phi_{,j}\frac{\partial x_j}{\partial \vartheta}\mathrm{d}\Omega+\int_\Omega w_2\frac{\partial \mathrm{d}\Omega}{\partial \vartheta}\\ &=\int_\Omega\left(w_2\frac{\partial x_j}{\partial \vartheta}\right)_{,j}\mathrm{d}\Omega=\int_S w_2\frac{\partial x_j}{\partial \vartheta}n_j\mathrm{d}S.\end{aligned}\tag{24}$$

By substituting Eq. (24) into Eq. (23), we can obtain

$$\begin{aligned}\frac{\partial \bar{W}}{\partial \vartheta} &= \int_{S_\phi}\left(\frac{\partial w_1}{\partial \phi}-\frac{\partial \gamma}{\partial n}\right)\frac{\partial \phi}{\partial \vartheta}\mathrm{d}S+\int_{S_q}\left(\frac{\partial w_1}{\partial q}+\gamma\right)\frac{\partial q}{\partial \vartheta}\mathrm{d}S\\ &+\int_S\left(\gamma_{,j}q+\frac{\partial \gamma}{\partial n}\phi_{,j}-\gamma_{,l}\phi_{,l}n_j+k^2\gamma\phi n_j\right)\frac{\partial x_j}{\partial \vartheta}\mathrm{d}S\\ &+\int_S\left(w_1+\gamma q\right)\frac{\partial \mathrm{d}S}{\partial \vartheta}+\int_S w_2\frac{\partial x_j}{\partial \vartheta}n_j\mathrm{d}S.\end{aligned}\tag{25}$$

Obviously, Eq. (25) does not contain the unknown sensitivity values of sound pressure and normal derivative on the boundary. However, it is noted that the boundary gradients of sound pressure and adjoint function γ are introduced in the sensitivity equation of the objective function. As the BEM is employed in this study, the boundary gradients of sound pressure can be calculated by differentiating Eq. (8) with respect to the coordinate.

It is noticed that the adjoint problem in Eq. (20) is analogous to the acoustic prediction problem, but with different boundary conditions and source term. So, the boundary integral equations and the solution procedures for the adjoint solution are very similar to those for acoustic problem. However, because of the source term in Eq. (20), we need to carry out integrals in the domain as well as on the boundary when solving the boundary integrals for the adjoint problem.

4 Numerical Examples

4.1 Element Types and Surface Error

The approach of continuous linear and quadratic boundary elements is often applied. Discontinuous higher-order boundary elements are developed to achieve higher accuracy [22–24]. It is well-known that interpolation nodes are located inside the element and the expressions of the interpolation functions are dependent on the position of the node inside the element, see Fig. 1. In this figure, 'DBEmn' and 'CBEmn' denote discontinuous boundary element and continuous boundary element with 'm' geometry nodes and 'n' interpolation nodes, respectively. For example 'DBE21' in Fig. 1 is the constant boundary element with two geometrical nodes denoting that linear shape functions exist, and 'DBE22' is discontinuous linear boundary element with two geometrical nodes. 'CBE22' element is used to be continuous linear boundary element, and 'CBE33' element is quadratic continuous boundary element. For detailed error comparison between 3D continuous boundary element and 3D discontinuous boundary element, please see paper [24]. For constant boundary element, the interpolation node is defined at the centroid of the element. For discontinuous linear boundary element, the values of a decide the position of these interpolation nodes. In this paper, the error function for the surface error based on the complex values is expressed as [24].

$$||e^\Gamma(x^j)|| = ||\phi_e(x^j)-\phi_n(x^j)||,\quad x\in\Gamma,\tag{26}$$

where ϕ_e represents the exact solution for the sound pressure, and ϕ_n the numerical solution. The discrete error function is evaluated in discrete points, and the discrete surface error is determined as

$$||e^\Gamma||_2=\left(\frac{1}{n}\sum_{j=1}^{n}||e^\Gamma(x^j)||^2\right)^{1/2},\tag{27}$$

where n represents the number of nodes on the surface Γ. And then, we use the relative error e_2^Γ for the sound pressure error

$$e_2^\Gamma=\frac{||e^\Gamma||_2}{||\phi_e^\Gamma||_2},\tag{28}$$

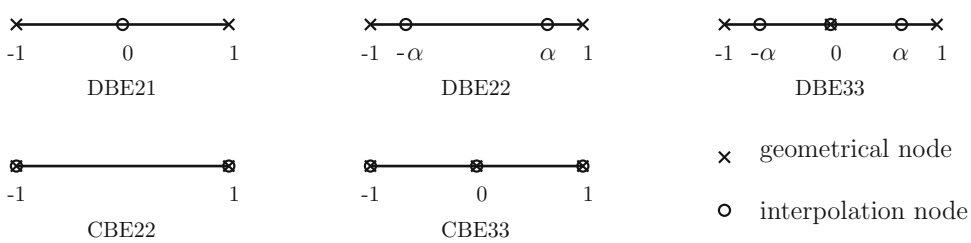

Fig. 1 Distribution of geometrical nodes and interpolation nodes

where $||\phi_e^{\Gamma}||_2$ represents the discrete Euclidean norm of the exact sound pressure, and can be expressed as the following formula

$$||\phi_e^{\Gamma}||_2 = \left(\frac{1}{n} \sum_{j=1}^{n} ||\phi_e(x^j)||^2 \right)^{1/2}. \tag{29}$$

4.2 Scattering from an Infinite Rigid Cylinder

A numerical simulation of acoustic scattering from an infinite rigid cylinder with Neumann boundary condition is given to demonstrate the accuracy and efficiency of the present algorithm. The computation is done on a desktop PC with an Pentium 2.59 GHz processor and 3.24 GB memory.

In this example, we consider the acoustic scattering of a plane incident wave with unit amplitude on an infinite rigid cylinder with radius $a = 1.0$m centred at point $(0, 0)$, and the plane incident wave is travelling along the positive x-axis ($\theta = 0$). The analytical solution of the sound pressure at point (r, θ) is given as

$$\phi(r, \theta) = -\sum_{n=0}^{\infty} \varepsilon_n i^n \frac{J_n'(ka)}{H_n^{(1)\prime}(ka)} H_n^{(1)}(kr) \cos(n\theta), \tag{30}$$

where ε_n denotes the Neumann symbols, i.e. $\varepsilon_0 = 1$; $\varepsilon_n = 2$ when n is greater than 0. $()'$ stands for the differentiation with respect to ka.

When the design variable is chosen as a, one can obtain the analytical solution of sound pressure sensitivity by differentiating Eq. (30) with respect to the design variable, as follows:

$$\frac{\partial \phi(r, \theta)}{\partial a} = -\sum_{n=0}^{\infty} \varepsilon_n i^n \left[\frac{J_n'(ka)}{H_n^{(1)\prime}(ka)} \right]' H_n^{(1)}(kr) \cos(n\theta). \tag{31}$$

Sample internal points are evenly distributed on a circle with radius $r = 2a$ and the coordinates of the computing point are $(2a, 0)$. In the procedure of FMM , the boundary of the circle is discretized with 80000 elements and the maximum number of boundary elements per leaf is set to 60. With this parameter, the number of tree levels is 10, the number of leaves is 2196 and the number of cells is 3829.

In Fig. 2, "analytical" denotes the analytical solution of acoustic pressure sensitivity, and "numerical" denotes the results obtained by numerical methods. DBE33 element is used for the numerical solution. From this figure, it can be seen that the numerical solution is in good agreement with the analytical solution at points located on circle $r = 2a$ with wave number $k = 1$, and it denotes the correctness and validity of the proposed algorithm.

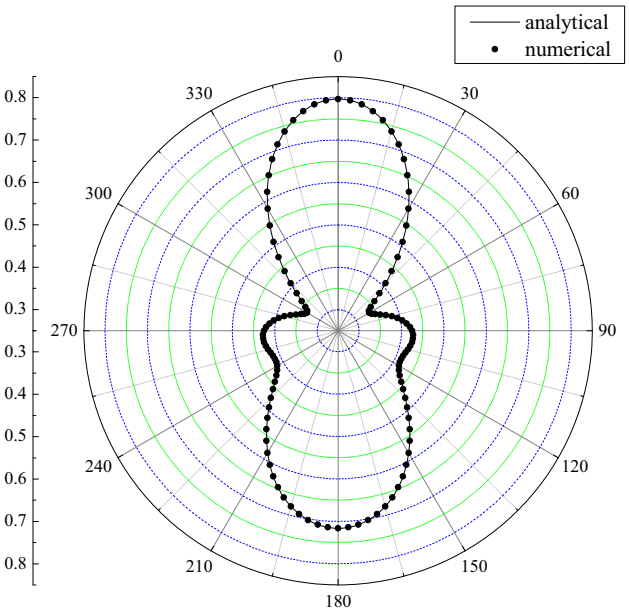

Fig. 2 Acoustic pressure sensitivity at points on circle $r = 2a$ with k = 1

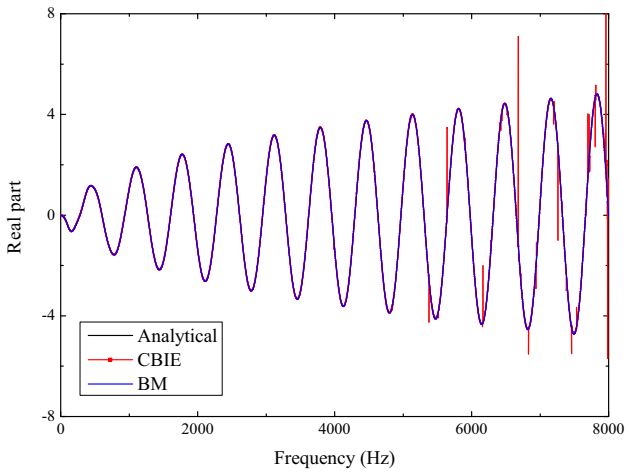

Fig. 3 Real part of acoustic pressure sensitivity at the computing point with different frequencies

Figures 3 and 4 show that the acoustic pressure sensitivity values obtained by CBIE have a big deviation from the analytical solution at fictitious frequencies, but the values obtained by Burton–Miller formulation is in good agreement with the analytical solutions. The CPU time used to calculate the sensitivity values at the computing point is plotted in Fig. 5, which demonstrates the efficiency of fast multipole boundary element method (FMBEM) for two-dimensional acoustic design sensitivity analysis.

For discontinuous boundary elements, the interpolation nodes are located inside the element, and the performance with a moving position is investigated in detail. Figure 6 shows the surface error in terms of nodal position for DBE22.

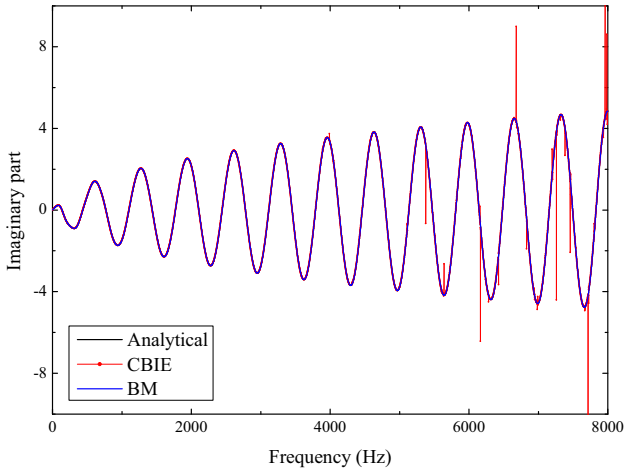

Fig. 4 Imaginary part of acoustic pressure sensitivity at the computing point with different frequencies

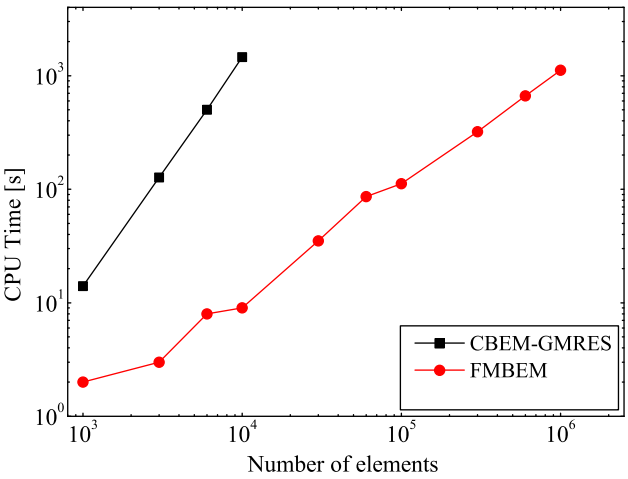

Fig. 5 CPU time used to calculate the pressure sensitivity values at the computing point with $f = 1000$ Hz

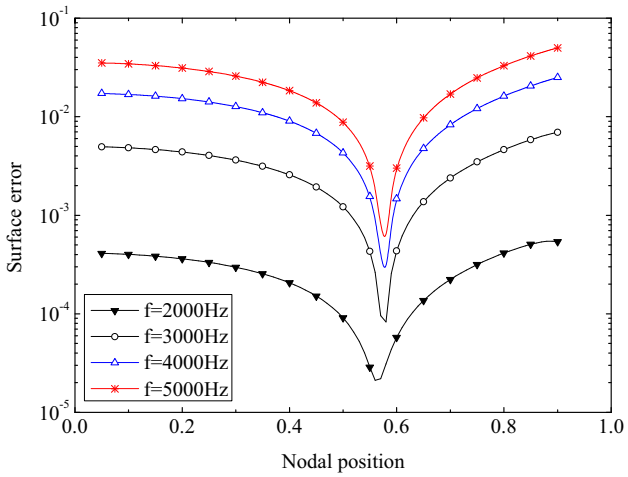

Fig. 6 Surface error in terms of nodal position for DBE22 element

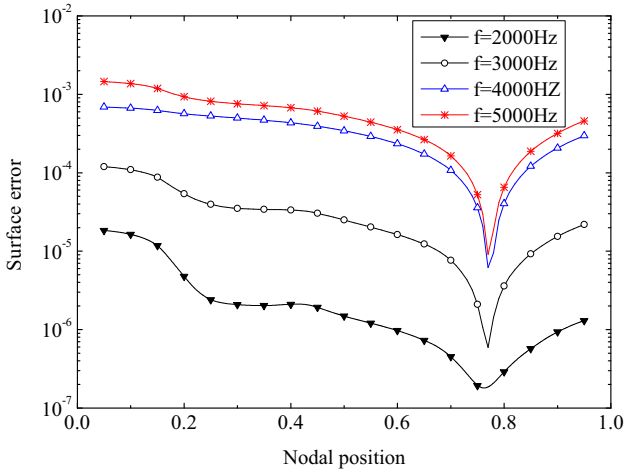

Fig. 7 Surface error in terms of nodal position for DBE33 element

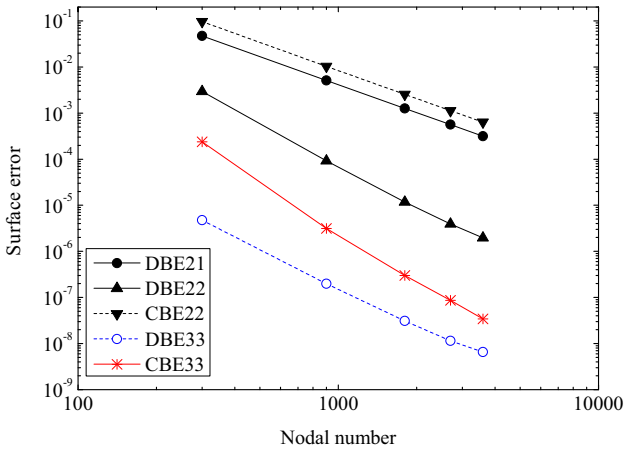

Fig. 8 Surface error of acoustic pressure sensitivity for different types of elements with $f = 1000$Hz

The step size for nodal position parameter is set as 0.01. From this figure, it can be seen that the surface error increases with frequency increases, and the optimal value of nodal position has a very small deviation with frequency, and all around 0.58 which is close to the zeros of the Legendre polynomial 0.5773. Figure 7 shows the surface error in terms of nodal position for DBE33 element. From this figure, it can be seen that the optimal values of nodal position for different error curves are all around 0.77 which is also close to the zeros of the Legendre polynomial 0.7746.

The performance of different types of elements is compared at similar computational cost. From Fig. 8, it can be seen that continuous element CBE22 performs the most inefficiently, and discontinuous element DBE33 with quadratic shape approximation performs the most efficiently. In addition, the discontinuous elements perform better than the continuous elements. Let us consider the convergence of numerical solution obtained using different types of boundary elements. Figure 9 shows the fitted curve for the five

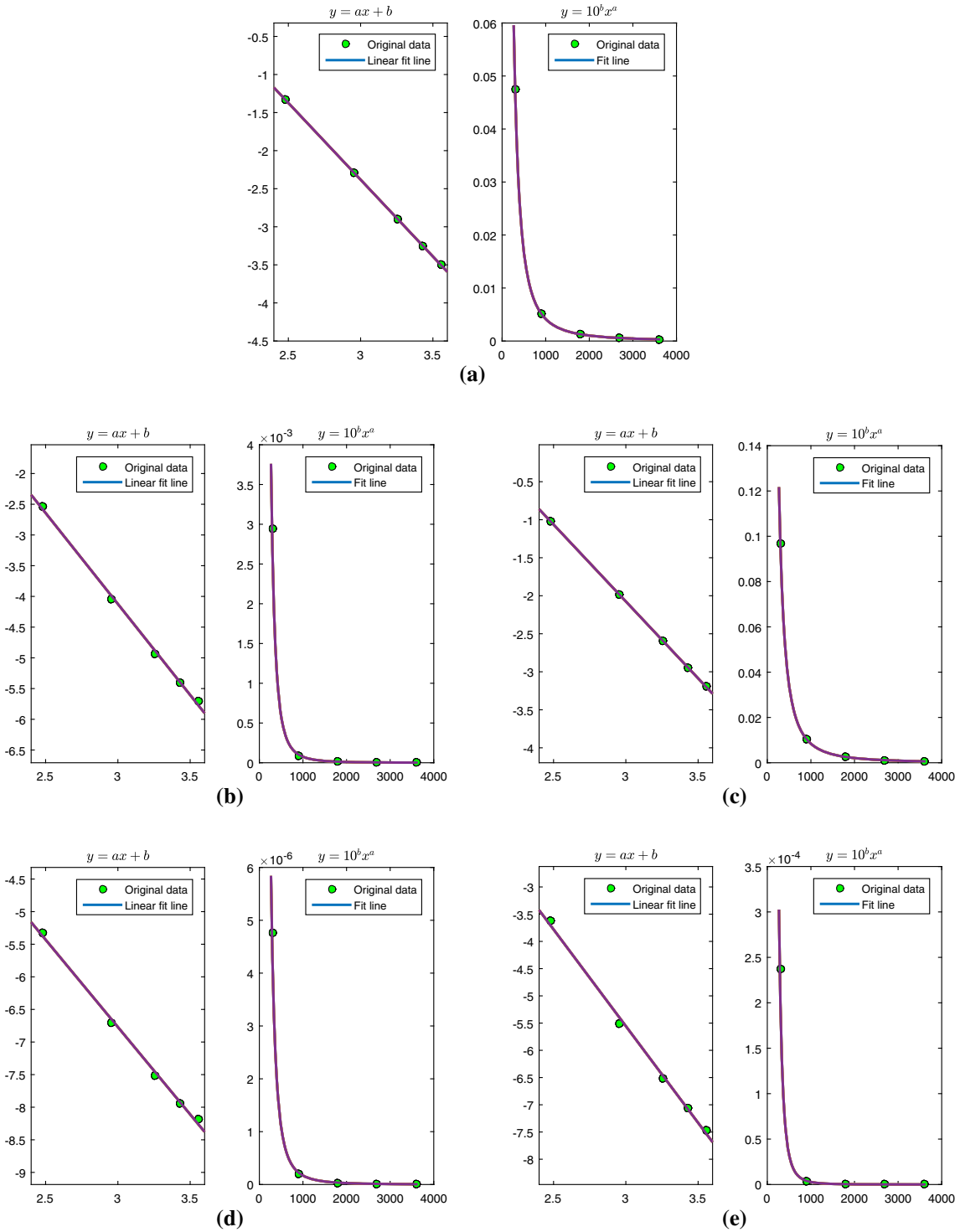

Fig. 9 Fitted curve for the relative error of sensitivity value

different boundary elements. The left figure in per subfigure denotes the linear fit line of the date showed in Fig. 8. The coefficients a and b for the linear fit line decide the relation between the surface error and the discrete element number in terms of logarithmic form. The right figure in per subfigure shows a good convergence of numerical solution. The

Table 1 The value of the coefficient a and b for different types of boundary element

	DBE21	DBE22	CBE22	DBE33	CBE33
a	−2.017	−2.962	−2.023	−2.680	−3.551
b	3.669	4.762	3.994	1.269	5.097

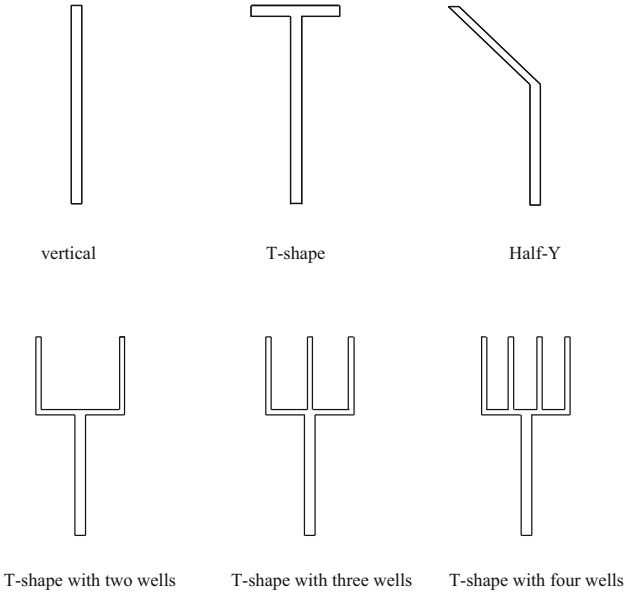

Fig. 10 Noise barriers with different top

surface error can be expressed as a function of discrete element number, such as $y = 10^b x^a$. Table 1 shows the value of the coefficients a and b for different types of boundary elements.

4.3 Scattering from Sound Barriers

Noise from expressways and railways is an important aspect of noise pollution but can be rectified by erecting barriers between the noise source and the zone to be protected [29]. For a long straight barrier and a line source, two-dimensional model can be used to predict the acoustic field. The barrier is assumed to have infinite length and its cross section is uniform along the length. In this example, several types of barriers that are erected on a rigid, flat and sufficient large ground are examined, see Fig. 10. Figure 11 shows cross-sectional contours of Y-shaped noise barrier over a plane ground at a distance of 10.5 m from a coherent homogeneous monofrequency line source situated 1.0 m above the ground. The width d of the barriers is set to 0.2 m. The source frequency is 100 Hz and all surfaces of the barriers are rigid. The vertical barrier is discretized with 120,000 elements with equal length, the T-shaped barrier 138,000 elements and the Half-Y-shaped barrier 124,230 elements. The coordinate of the six sample points are (15, 2), (30, 2), (45, 2), (15, 5), (30, 5), and (45, 5).

Figure 12 shows the sound pressure-level distribution for the case of a vertical barrier, then T-shaped barrier in Fig. 13 and Half-Y-shaped barrier with angle $\theta = 40°$ in Fig. 14. Absorbing material is used to improve the performance of the noise barriers. In the three figures, the surface admit-

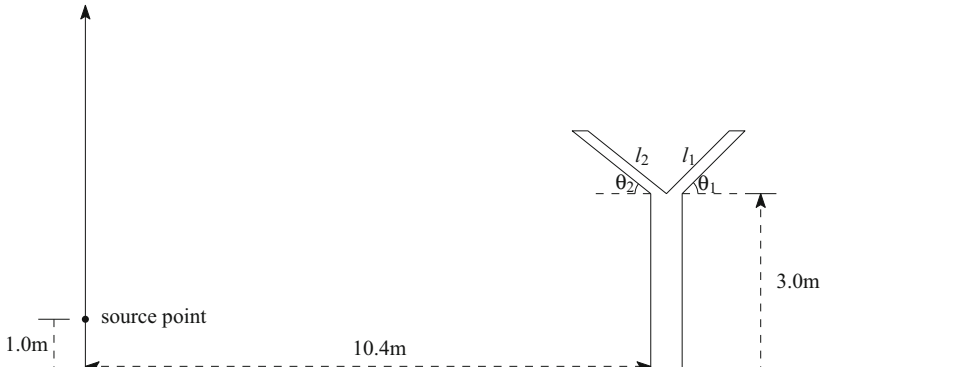

Fig. 11 Cross section of the Y-shaped noise barrier

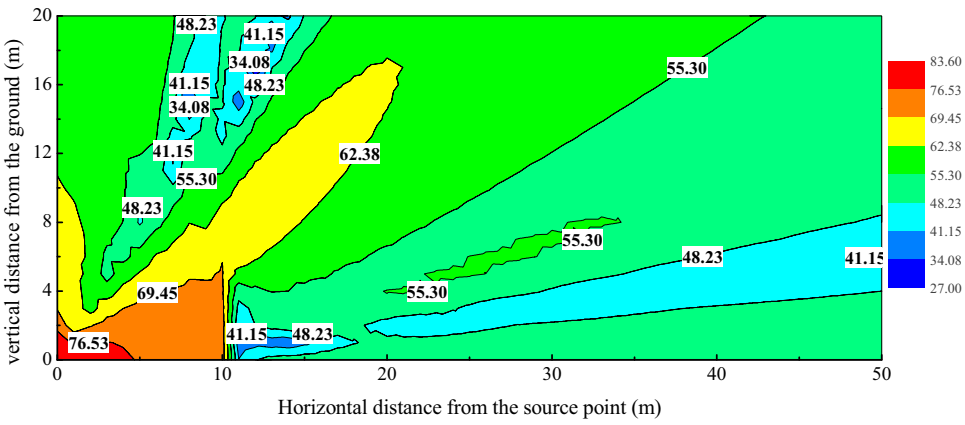

Fig. 12 Noise-level distribution around a vertical barrier (db)

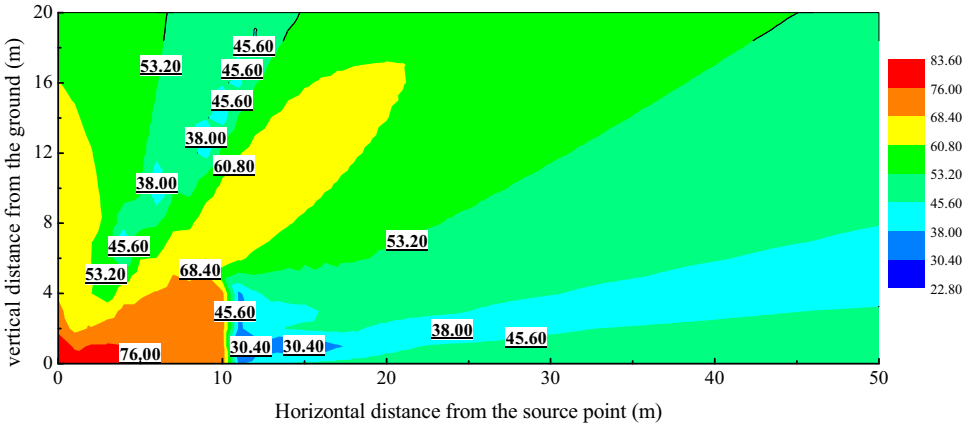

Fig. 13 Noise-level distribution around a T-barrier (db)

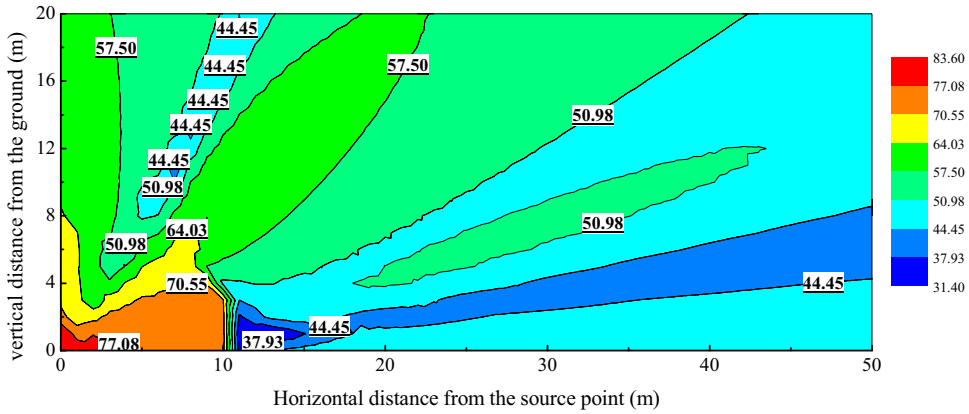

Fig. 14 Noise-level distribution around a Half-Y-shaped barrier (db)

Table 2 The sound pressure level at sample points for T-shaped noise barriers with a series of wells

T-shape	(15, 2)	(30, 2)	(45, 2)	(15, 5)	(30, 5)	(45, 5)	Mean	δIL
2 wells	38.91	40.93	44.94	46.88	47.48	38.40	42.92	0
3 wells	36.80	38.73	43.17	45.28	46.06	37.23	41.21	−1.71
4 wells	36.57	38.44	42.97	45.07	45.93	37.03	41.00	−1.92
5 wells	36.46	38.31	42.88	44.97	45.87	36.94	40.91	−2.02
6 wells	36.40	38.24	42.83	44.92	45.84	36.89	40.85	−2.07
7 wells	36.36	38.18	42.79	44.88	45.82	36.86	40.82	−2.11

tance is set to 1.0. From the above three figures, one can find that T-shaped and Half-Y noise barriers perform more efficiently than vertical noise barrier, and it denotes that adding substructures at the top of noise barriers has the advantage of improving the barrier performance without increasing its overall height.

The performance of T-shaped noise barriers with a series of wells is compared in Table 2. The whole height is 5 m, the height of the bottom is 3 m, the height of the top is 2 m, and the length of the top is 2 m. The thickness of the wells on the top is 0.03 m. Absorbing material is used to improve the performance of the noise barriers. In this example, the surface admittance is set to 1.0. Table 2 shows that the noise barrier with more wells produces smaller sound pressure level. The

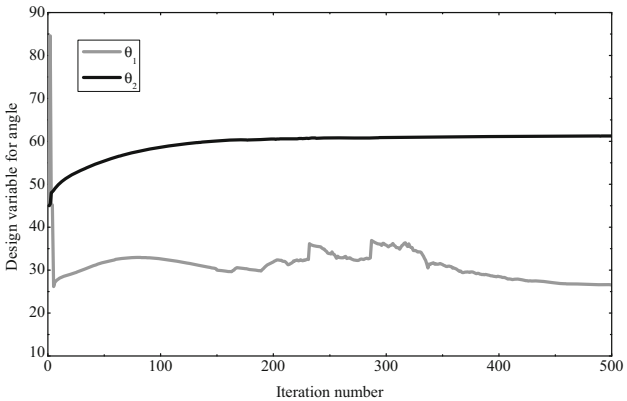

Fig. 15 Values of θ_1 and θ_2 with number of iteration

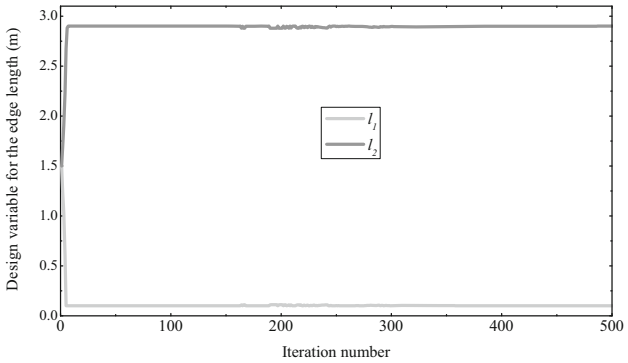

Fig. 16 Values of l_1 and l_2 with number of iteration

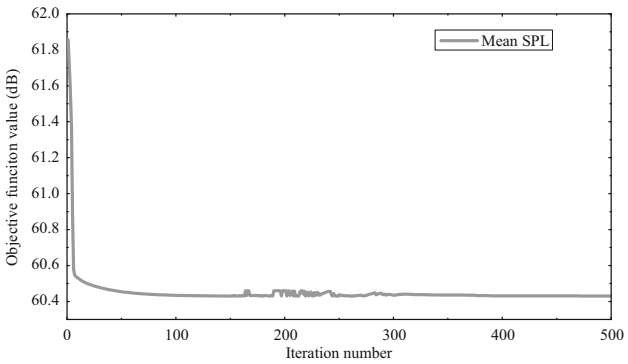

Fig. 17 Values of objective function with number of iteration

mean sound pressure level for the noise barrier with 3 wells decreases 1.71 dB than that for the barrier with 2 wells, and then 1.92, 2.02, 2.07, and 2.11 dB in sequence. More wells will not reduce significantly the sound pressure level, but need more material and take high cost. In sum, the T-shaped noise barrier with 3 wells performs the most efficiently.

In this section, MMA [30] is introduced for the shape optimization of Y-shaped noise barrier. In optimization process, the angle θ_1, θ_2, and the length l_1, l_2 in Fig. 11 are chosen to be the design variables. The objective function, to be minimized, is the mean sound pressure level at the sample points.

subject to

$$l_1 + l_2 \leq 3.0 \tag{32}$$

and

$$0 \leq \theta_k \leq 90, \quad k = 1, 2; \qquad 0 \leq l_k \leq 3, \quad k = 1, 2 \tag{33}$$

initial values of design variables

$$\theta_1 = \theta_2 = 45; \qquad l_1 = l_2 = 1.5. \tag{34}$$

Figures 15, 16 and 17 show that the design variables and objective functions change with the iteration number, and then converge in 500 iteration. The optimal value of the objective function approaches to 60.42 dB. The optimal value of design variable is $\theta_2 = 62°$, $\theta_1 = 27°$. Because of the limitation of $l_1 > 0.1$ which is demanded to discrete the edge, the optimal value of l_1 approaches to the minimum value. Actually, the optimal value of l_1 approaches to zero when the minimum value of l_1 approaches to zero. Similarly, the optimal value of l_2 approaches to 3. This result denotes that the Y-shaped noise barrier after optimization becomes the half-Y noise barrier. So, half-Y noise barrier performs more efficiently than Y-shaped noise barrier. Figure 18 shows the SPL contour plot of half-Y barrier with frequency $f = 200$ Hz. The sensitivity value of objective function needs to be solved in per iteration step for optimization analysis, and adjoint variable method is used to solve the sensitivity value in this paper. In addition, this step needs much more time in the optimization analysis. However, the application of FMM can improve significantly the efficiency of optimization analysis.

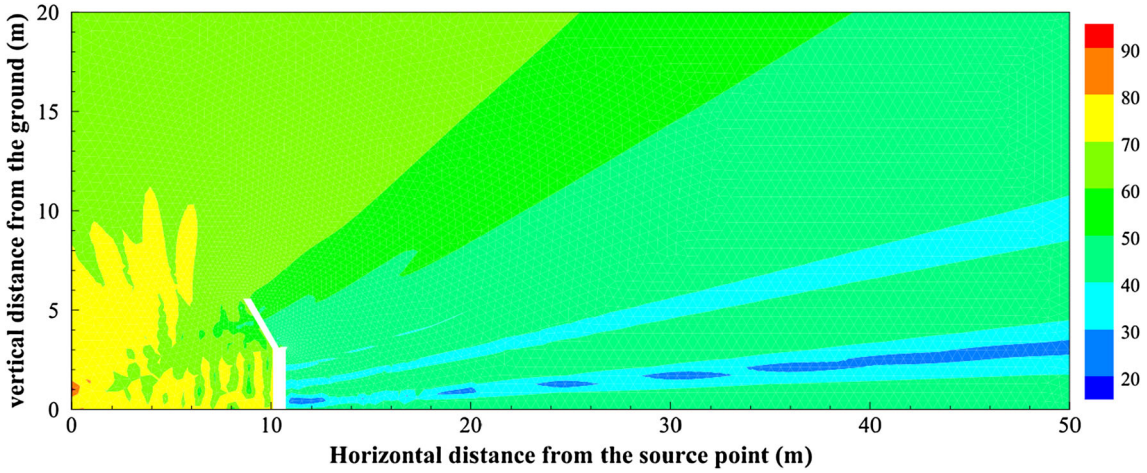

Fig. 18 SPL contour plot of half-Y noise barrier

5 Conclusion

A novel algorithm based on discontinuous boundary elements is presented for the simulation of acoustic scattering. The Burton–Miller method is used to obtain correct solutions at all frequencies. The strong singular integral for different types of boundary elements is evaluated explicitly and directly with Cauchy principal value and the Hadamard finite part integral method. An example with analytical solution is presented to demonstrate the correctness and validity of the proposed algorithm, and the performance of different types of elements is presented and compared. The result that the nodal position for discontinuous boundary elements has a big impact on the numerical performance is presented, and the optimal nodal position values are also given in this paper. Adjoint variable method is used to solve the sensitivity value of objective function, and MMA is used for the optimization analysis. At last, the example of scattering from the sound barriers is presented to demonstrate the availability of the proposed algorithm.

Compliance with Ethical Standards

Conflict of Interest We declare that we have no conflict of interest.

Funding This study was funded by the National Natural Science Foundation of China (Grant nos. 11172291, and U1504505).

Appendix 1: Evaluation of the Integrals on S_ε and Γ_ε

After piecewise discretization, the CBIE and NDBIE formulas can be rewritten as

$$\frac{1}{2}\phi(x^j)+B(x^j)=\int_{S\setminus S_{xj}} G(x^j,x)q(x)\mathrm{d}S(x) - \int_{S\setminus S_{xj}} F(x^j,x)\phi(x)\mathrm{d}S(x), \tag{35}$$

and

$$\frac{1}{2}q(x^j)+D(x^j)=\int_{S\setminus S_{xj}} G^1(x^j,x)q(x)\mathrm{d}S(x) - \int_{S\setminus S_{xj}} F^1(x^j,x)\phi(x)\mathrm{d}S(x), \tag{36}$$

$S\setminus S_{xj}$ denotes the boundary S except S_{xj}, S_{xj} is the element containing the source point x^j. S_ε denotes a semi-circle with a radius ε centred at x^j and Γ_ε denotes $S_{xj}\setminus S_\varepsilon$.

The function $f(x)$ in every boundary element can be expressed as the following formulation

$$f(x)=\sum_{k=1}^{m}\Phi_k f(x^k), \tag{37}$$

where m denotes the number of interpolation nodes in every boundary element, Φ denotes the interpolation function. Function $f(x)$ could be chosen as $\phi(x)$, $q(x)$ and so on.

1. For constant element
   $m=1$ and $\Phi=1$.
2. For linear element

$$\Phi_1=\frac{1}{2}\left(1-\frac{\xi}{\beta}\right),\quad \Phi_2=\frac{1}{2}\left(1+\frac{\xi}{\beta}\right), \tag{38}$$

   where ξ means the local coordinate of the point x, and β denotes the position of interpolation nodes on the discontinuous element. When $\beta=1$, Eq. (38) denotes expression of the interpolation functions for linear continuous element.
3. For quadratic element.

$$\Phi_1=\frac{\xi}{2\beta}\left(\frac{\xi}{\beta}-1\right),\quad \Phi_2=1-\frac{\xi^2}{\beta^2},\quad \Phi_3=\frac{\xi}{2\beta}\left(\frac{\xi}{\beta}+1\right). \tag{39}$$

Using Eq. (37) , one can obtain the expression of the coordinate (x_1,x_2) at the point x, as follows

$$x_1(\xi)=\frac{1}{2}A_1\xi^2+A_2\xi+x_1^b, \tag{40}$$

$$x_2(\xi)=\frac{1}{2}A_3\xi^2+A_4\xi+x_2^b, \tag{41}$$

where $x_k^b(k=1,2)$ denotes the coordinate of the central point in the boundary element, and the coefficient $A_k(k=1,4)$ can be derived by

$$A_1=x_1^c-2x_1^b+x_1^a,\quad A_2=\frac{1}{2}(x_1^c-x_1^a),\quad A_3=x_2^c-2x_2^b+x_2^a,\quad A_4=\frac{1}{2}(x_2^c-x_2^a), \tag{42}$$

where $x_k^a(k=1,2)$ and x_k^c denotes the coordinate of the two extreme points in the boundary element. Similar as linear element, Eq. (39) denotes expression of the interpolation functions for quadratic continuous element when $\beta=1$.

When different types of elements are used to discretize the boundary, one can obtain the different expression of coefficient $B(x^j)$ and $D(x^j)$ in Eqs. (35) and (36), as follows

1. For constant element

$$B(x^j) = -C_1 q(x^j), \tag{43}$$
$$D(x^j) = -C_2 \phi(x^j), \tag{44}$$

where coefficient C_1 and C_2 can be expressed as the following formulation

$$C_1 = -\frac{L}{2\pi}\left[\ln(\frac{kL}{2}) - 1\right] + \frac{\mathrm{i}}{4}\lim_{\varepsilon\to 0}\int_{\Gamma_\varepsilon}\left[H_0^{(1)}(kr) - \frac{2\mathrm{i}}{\pi}\ln(kr)\right]\mathrm{d}S(y), \tag{45}$$

$$C_2 = \frac{\mathrm{i}k^2}{4}\lim_{\varepsilon\to 0}\int_{\Gamma_\varepsilon}\left[\frac{H_1^{(1)}(kr)}{kr} + \frac{2\mathrm{i}}{\pi k^2 r^2} - \frac{\mathrm{i}}{\pi}\ln(kr)\right]\mathrm{d}S(y) - \frac{k^2 L}{4\pi}\left[\ln\left(\frac{kL}{2}\right) + \frac{8}{k^2L^2} - 1\right], \tag{46}$$

where L is the length of the element in which node x^j locates.

2. For linear element

$$B(x^j) = -\left[B_1 q(x^j) + B_2 q(x^l)\right], \tag{47}$$
$$D(x^j) = -\left[D_1 \phi(x^j) + D_2 \phi(x^l)\right], \tag{48}$$

where point x^l is the another node located on a boundary element containing node x^j. α denotes the local coordinate of the node x^j, and $\beta = |\alpha|$. For linear discontinuous boundary element ($\beta \neq 1$), coefficients B_1, B_2, D_1 and D_2 are expressed as following

$$B_1 = \frac{\mathrm{i}L}{8}\int_{-1}^{1}\left[H_0^1(kr) - \frac{2\mathrm{i}}{\pi}\ln(kr)\right]\phi_1\,\mathrm{d}\xi - \frac{L}{2\pi}\ln\frac{kL}{2} - \frac{L}{8\pi\beta}II_1, \tag{49}$$

$$B_2 = \frac{\mathrm{i}L}{8}\int_{-1}^{1}\left[H_0^1(kr) - \frac{2\mathrm{i}}{\pi}\ln(kr)\right]\phi_2\,\mathrm{d}\xi - \frac{L}{2\pi}\ln\frac{kL}{2} - \frac{L}{8\pi\beta}II_2, \tag{50}$$

$$D_1 = \frac{\mathrm{i}k^2 L}{8}\int_{-1}^{1}\left[\frac{H_1^1(kr)}{kr} + \frac{8\mathrm{i}}{\pi k^2 L^2}\frac{1}{(\xi-\alpha)^2} - \frac{\mathrm{i}}{\pi}\ln(kr)\right]\mathrm{d}\xi + \frac{\ln(1+\beta) - \ln(1-\beta)}{2\beta\pi L} - \frac{k^2 L}{4\pi}\ln\frac{kL}{2} - \frac{k^2 L}{8\pi}II_1 \tag{51}$$

$$D_2 = \frac{\mathrm{i}k^2 L}{8}\int_{-1}^{1}\left[\frac{H_1^1(kr)}{kr} + \frac{8\mathrm{i}}{\pi k^2 L^2}\frac{1}{(\xi-\alpha)^2} - \frac{\mathrm{i}}{\pi}\ln(kr)\right]\mathrm{d}\xi + \frac{\ln(1+\beta) - \ln(1-\beta)}{2\beta\pi L} - \frac{2}{\pi L(1-\beta^2)} - \frac{k^2 L}{4\pi}\ln\frac{kL}{2} - \frac{k^2 L}{8\pi}II_2, \tag{52}$$

where

$$r(\xi) = \frac{L}{2}|\xi - \alpha|, \tag{53}$$

$$II_1 = \int_0^{1+\beta} x\ln x\,\mathrm{d}x - \int_0^{1-\beta} x\ln x\,\mathrm{d}x, \tag{54}$$

$$II_2 = \int_0^{1-\beta}\ln x\,\mathrm{d}x + \int_0^{1+\beta}\ln x\,\mathrm{d}x - \frac{1}{2\beta}\left(\int_0^{1+\beta} x\ln x\,dx - \int_0^{1-\beta} x\ln x\,\mathrm{d}x\right). \tag{55}$$

For linear continuous boundary element ($\beta = 1$), coefficients B_1, B_2, D_1 and D_2 are expressed as following

$$B_1 = \frac{\mathrm{i}L}{8}\int_{-1}^{1}\left[H_0^1(kr) - \frac{2\mathrm{i}}{\pi}\ln(kr)\right]\phi_1\,\mathrm{d}\xi - \frac{L}{8\pi}(2\ln(kL) - 3), \tag{56}$$

$$B_2 = \frac{\mathrm{i}L}{8}\int_{-1}^{1}\left[H_0^1(kr) - \frac{2\mathrm{i}}{\pi}\ln(kr)\right]\phi_2\,\mathrm{d}\xi - \frac{L}{8\pi}(2\ln(kL) - 1), \tag{57}$$

$$D_1 = \frac{\mathrm{i}k^2 L}{8}\int_{-1}^{1}\left[\frac{H_1^1(kr)}{kr} + \frac{2\mathrm{i}}{\pi k^2 r^2} - \frac{\mathrm{i}}{\pi}\ln(kr)\right]\phi_1\,\mathrm{d}\xi - \frac{1}{2\pi L}(1+\ln 2) - \frac{k^2 L}{16\pi}(2\ln(kL) - 3), \tag{58}$$

$$D_2 = \frac{\mathrm{i}k^2 L}{8}\int_{-1}^{1}\left[\frac{H_1^1(kr)}{kr} + \frac{2\mathrm{i}}{\pi k^2 r^2} - \frac{\mathrm{i}}{\pi}\ln(kr)\right]\phi_2\,\mathrm{d}\xi + \frac{\ln 2}{2\pi L} - \frac{k^2 L}{16\pi}(2\ln(kL) - 1). \tag{59}$$

3. For quadratic element

$$B(x^j) = -\left[B_1 q(x^j) + B_2 q(x^l) + B_3 q(x^m)\right], \tag{60}$$
$$D(x^j) = -\left[D_1 \phi(x^j) + D_2 \phi(x^l) + D_3 \phi(x^m)\right], \tag{61}$$

where points x^l and x^m are the other nodes that are located on a boundary element containing node x^j. For quadratic discontinuous boundary element ($\beta \neq 1$), coefficients

B_1, B_2, B_3, D_1, D_2, D_3 are expressed as following

$$B_m = \frac{\mathrm{i}}{4}\int_{-1}^{1}\phi_m\Big[H_0^1(kr)J_1 - \frac{2\mathrm{i}}{\pi}\ln(kr_1)J_2\Big]\,\mathrm{d}\xi - \frac{J_2}{2\pi}(\ln k + \ln J_2)\int_{-1}^{1}\phi_m\,\mathrm{d}\xi - \frac{J_2}{2\pi}\int_{-1}^{1}\phi_m \ln|\xi-\alpha|\,\mathrm{d}\xi, \quad m = 1, 2, 3, \tag{62}$$

$$D_m = \frac{\mathrm{i}k^2}{4}\int_{-1}^{1}\phi_m\Big[\frac{H_1^1(kr)}{kr}n_j(x)n_j(y)J_1(\xi) + \frac{2\mathrm{i}}{\pi k^2}\frac{1}{(\xi-\alpha)^2 J_2} - \frac{\mathrm{i}}{\pi}\ln(kr_1)J_2\Big]\,\mathrm{d}\xi - \frac{k^2 J_2}{4\pi}(\ln k + \ln J_2)\int_{-1}^{1}\phi_m\,\mathrm{d}\xi + \frac{1}{2\pi J_2}\int_{-1}^{1}\frac{\phi_m}{(\xi-\alpha)^2}\mathrm{d}\xi - \frac{k^2 J_2}{4\pi}\int_{-1}^{1}\phi_m \ln|\xi-\alpha|\,\mathrm{d}\xi, \quad m = 1, 2, 3, \tag{63}$$

where

$$r^2 = (\xi-\alpha)^2\left\{\left[\frac{1}{2}A_1(\xi+\alpha)+A_2\right]^2 + \left[\frac{1}{2}A_3(\xi+\alpha)+A_4\right]^2\right\}, \tag{64}$$

$$r_1^2 = (\xi-\alpha)^2 J_2^2, \tag{65}$$

$$J_1^2 = (A_1\xi + A_2)^2 + (A_3\xi + A_4)^2, \tag{66}$$

$$J_2^2 = (A_1\alpha + A_2)^2 + (A_3\alpha + A_4)^2. \tag{67}$$

When $\beta = 1$, the coefficients B_m and D_m for quadratic continuous element can be obtained using Eqs. (62) and (63).

References

1. Marburg, S.: Developments in structural-acoustic optimization for passive noise control. Arch. Comput. Methods Eng. **27**, 291–370 (2002)
2. Ratle, A., Berry, A.: Use of genetic algorithms for the vibroacoustic optimization of a plate carrying point-masses. J. Acoust. Soc. Am. **104**, 3385–3397 (1998)
3. Shojaeifard, M.H., Talebitooti, R., Yadollahi, A.: Optimization of sound transmission through laminated composite cylinderical shells using a genetic algorithm. Mech. Compos. Mater. **47**, 481–494 (2011)
4. Hambric, S.A.: Approximation techniques for broad-band acoustic radiated noise design optimization problems. J. Vib. Acoust. **117**, 136–144 (1995)
5. Tinnsten, M., Carlsson, P., Jonsson, M.: Stochastic optimization of acoustic response—a numerical and experimental comparison. Struct. Multidiscipl. Optim. **23**, 405–411 (2002)
6. van Houten, M.H.: Function Approximation Concepts for Multidisciplinary Design Optimization. Dissertation, Technische Universiteit Eindhoven (1998)
7. Ranjbar, M., Hardtke, H.-J., Fritze, D., Marburg, S.: Finding the best design within limited time: a comparative case study on methods for optimization in structural acoustics. J. Comput. Acoust. **18**, 149–164 (2010)
8. Lamancusa, J.S.: Numerical optimization techniques for structural-acoustic design of rectangular panels. Compos. Struct. **48**, 661–675 (1993)
9. Hambric, S.A.: Sensitivity calculations for broad-band acoustic radiated noise design optimization problems. J. Vib. Acoust. **118**, 529–532 (1996)
10. Marburg, S., Hardtke, H.-J.: Shape optimization of a vehicle hatshelf: improving acoustic properties for different load-cases by maximizing first eigenfrequency. Compos. Struct. **79**, 1943–1957 (2001)
11. Marburg, S., Hardtke, H.-J.: Efficient optimization of a noise transfer function by modification of a shell structure geometry. Part ii: Application to a vehicle dashboard. Struct. Multidiscipl. Optim. **24**, 60–71 (2002)
12. Haftka, R.T., Adelman, H.M.: Recent developments in structural sensitivity analysis. Struct. Optim. **1**, 137–151 (1989)
13. Marburg, S.: Efficient optimization of a noise transfer function by modification of a shell structure geometry. Part i: Theory. Struct. Multidiscipl. Optim. **24**, 51–59 (2002)
14. Chen, L.L., Chen, H.B., Zheng, C.J.: FEM/wideband FMBEM coupling for fluid-structure interaction problem and 2D acoustic design sensitivity analysis. CMES-Comput. Model. Eng. Sci. **94**(6), 459–483 (2013)
15. Chen, L.L., Zheng, C.J., Chen, H.B.: FEM/wideband FMBEM coupling for structural-acoustic design sensitivity analysis. Comput. Methods Appl. Mech. Eng. **276**, 1–19 (2014)
16. Chen, L.L., Chen, H.B., Zheng, C.J., Marburg, S.: Structural-acoustic sensitivity analysis of radiated sound power using a finite element/discontinuous fast multipole boundary element scheme. Int. J. Numer. Methods Fluids (2016). doi:10.1002/fld.4244
17. Choi, K.K., Shim, I., Wang, S.: Design sensitivity analysis of structure-induced noise and vibration. J. Vib. Acoust. **119**, 173–179 (1997)
18. Wang, S.: Design sensitivity analysis of noise, vibration and harshness of vehicle body structure. Mech. Struct. Mach. **27**, 317–336 (1999)
19. Chen, L.L., Zheng, C.J., Chen, H.B.: A wideband FMBEM for 2D acoustic design sensitivity analysis based on direct differentiation method. Comput. Mech. **52**, 631–648 (2013)
20. Zheng, C.J., Matsumoto, T., Takahashi, T., Chen, H.B.: Explicit evaluation of hypersingular boundary integral equations for acoustic sensitivity analysis based on direct differentiation method. Eng. Anal. Bound. Elem. **35**, 1225–1235 (2011)
21. Zheng, C.J., Matsumoto, T., Takahashi, T., Chen, H.B.: A wideband fast multipole boundary element method for three dimensional acoustic shape sensitivity analysis based on direct differentiation method. Eng. Anal. Bound. Elem. **36**, 361–371 (2012)
22. Rego Silva, J.J.D.: Acoustic and Elastic Wave Scattering Using Boundary Elements. Computational Mechanics Publications, Southampton (1993)
23. Tadeu, A., Antonio, J.: Use of constant, linear and quadratic boundary elements in 3d wave diffraction analysis. Eng. Anal. Bound. Elem. **24**, 131–144 (2000)
24. Marburg, S., Schneider, S.: Influence of element types on numeric error for acoustic boundary elements. J. Comput. Acoust. **11**, 363–386 (2003)

25. Marburg, S.: Six boundary elements per wavelength. Is that enough ? J. Comput. Acoust. **10**, 25–51 (2002)
26. Atkinson, K.E.: The Numerical Solution of Integral Equations of the Second Kind. Cambridge University Press, Cambridge (1997)
27. Burton, A.J., Miller, G.F.: The application of integral equation methods to the numerical solution of some exterior boundary-value problem. Proc. R. Soc. Lond. A **323**, 201–210 (1971)
28. Amini, S.: On the choice of coupling parameter in boundary integral formulations of the acoustic problem. Appl. Anal. **35**, 75–92 (1990)
29. Takashi, I., Kyoji, F.: Performance of noise barriers with various edge shapes and acoustical conditions. Appl. Acoust. **65**, 125–141 (2004)
30. Svanberg, K.: The method of moving asymptotes-a new method for structural optimization. Int. J. Numer. Meth. Eng. **24**, 359–373 (1987)